Separation Science and Technology
Publication details, including instructions for authors and subscription information:
http://www.informaworld.com/smpp/title~content=t713708471

Prediction of Dimensionless Cutsize for Size-Fractionated Measurements of Particles that Impact on a Sintered Stainless-Steel Filter

Cheng-Hsiung Huang[a]; Tser-Sheng Lin[a]; Sheh-Hsun Chang[b]; Chuen-Jinn Tsai[b]
[a] Department of Environmental Engineering and Health, Yuanpei University, Hsinchu, Taiwan [b] Institute of Environment Engineering, National Chiao Tung University, Hsinchu, Taiwan

To cite this Article Huang, Cheng-Hsiung , Lin, Tser-Sheng , Chang, Sheh-Hsun and Tsai, Chuen-Jinn(2007) 'Prediction of Dimensionless Cutsize for Size-Fractionated Measurements of Particles that Impact on a Sintered Stainless-Steel Filter', Separation Science and Technology, 42: 3, 477 — 491
To link to this Article: DOI: 10.1080/01496390601120656
URL: http://dx.doi.org/10.1080/01496390601120656

Separation Science and Technology, 42: 477–491, 2007

ISSN 0149-6395 print/1520-5754 online
DOI: 10.1080/01496390601120656

Prediction of Dimensionless Cutsize for Size-Fractionated Measurements of Particles that Impact on a Sintered Stainless-Steel Filter

Cheng-Hsiung Huang and Tser-Sheng Lin
Department of Environmental Engineering and Health, Yuanpei University, Hsinchu, Taiwan

Sheh-Hsun Chang and Chuen-Jinn Tsai
Institute of Environment Engineering, National Chiao Tung University, Hsinchu, Taiwan

Abstract: This investigation experimentally studied the penetration curve of particles that impact on a sintered stainless-steel filter with various pore sizes, sampling flow rates and jet diameters. The penetration curves were compared to those with an aluminum foil substrate. Test data reveal that when the sintered stainless-steel filter has larger pore sizes (100 μm or 40 μm), the particle penetration, P(%), is lower and the curve is less steep than that obtained from the aluminum foil substrate. The penetration curve of the sintered stainless-steel filter with smaller pore size (5 μm) is close to that of the aluminum foil substrate. The dimensionless cutsize-shift (the ratio of the dimensionless cutsize of sintered stainless-steel filter to that of aluminum foil) falls as the pore sizes and the Reynolds number increase. Experimental data were then compared with theoretical results, and theory over-predicted the dimensionless cutsize-shift. Hence, a regression equation for the dimensionless cutsize-shift is proposed by fitting the experimental data. The discrepancy between the experimental data and the regression prediction is within 4%. The regression equation can be used to predict the dimensionless cutsize for the size-fractionated measurements of

Received 1 August 2006, Accepted 22 October 2006
Address correspondence to Cheng-Hsiung Huang, Department of Environmental Engineering and Health, Yuanpei University, Hsinchu, Taiwan. Tel.: +886-3-6108534; Fax: +886-3-6102337; E-mail: chhuang@mail.ypu.edu.tw

particles that impact on a sintered stainless-steel filter with various sized pores and Reynolds numbers.

Keywords: Dimensionless cutsize, particle penetration, sintered stainless-steel filter

INTRODUCTION

Measurement of particle size distribution and chemical species in air stream is important to evaluate adverse effects on human health, visibility, climate, and ecosystems. Numerous inertial classifiers have been designed and used for particle size-fractionated measurement in the ambient and workplace environments (1–3). Particles deposited on the collection surfaces of the inertial classifiers can be weighed and analyzed further for chemical composition. However, some sampling artifacts including particle bounce, particle overloading, and particle blow-off may occur and affect the measured size distribution (4–6).

In order to conquer particle bounce, re-entrainment, and over-loading problems of the inertial classifiers, sintered stainless-steel filters have been used as the collection surfaces in classifying particles (7–10). The sintered stainless-steel filter can be utilized in an electrical low-pressure impactor (9). Diesel soot rapidly overloads the electrical low-pressure impactor when a standard flat-plat substrate is employed. The overloading problem has been eliminated using an oil-soaked sintered stainless-steel filter in the electrical low-pressure impactor (10). However, for a high-velocity jet, the use of the sintered stainless-steel filter saturated with low-viscosity oil is improperly, because the jet will easily blow the oil away (11). Accordingly, the sintered stainless-steel filters uncoated or impregnated with a little oil are frequently employed to collect samples. In addition, sintered stainless-steel filters are readily available, cleanable, reusable, and electrically conductive (11, 12). It is noteworthy that they can be also used to collect particles at high temperature and in corrosive environments (13).

The influence of porosity and surface roughness of a dry sintered stainless-steel filter on the particle collection efficiency of a cascade multi-jet low-pressure classifier has been experimentally studied, yielding findings which revealed that larger pores and rougher sintered stainless-steel filters were associated with smaller cutsizes and less sharp collection efficiency curves (9). Thus, re-calibration and even re-scaling of the inertial classifier with stainless-steel filters were needed. Recently, a simple theory was introduced to estimate the cutsize for particles that impact on a porous substrate (14, 15). The developed theoretical equation was the first approximation to predict the cutsize-shift (the ratio of the cutsize of the porous substrate to that of the normal substrate) for particles that impact on a stainless-steel filter. The approximation to the cutsize-shift may not apply for cases when the surface roughness of the porous substrate dominates the change in the particle collection efficiency (14).

This work seeks to determine experimentally the particle penetration curve of particles that impact on a sintered stainless-steel filter from a circular jet. The penetration curves obtained by using an aluminum foil were compared at various sampling flow rates ($1.5 \sim 4.5$ L/min) and jet diameters (0.26 and 0.36 cm). The experimental findings were compared with the theoretical results. Finally, a regression equation for the dimensionless cutsize-shift for particles that impact on a sintered stainless-steel filter was determined by fitting the experimental data.

THEORY

When a particle-laden stream from a jet impacts on a stainless-steel porous filter, the stream penetrates into the porous filter and shifts the particle penetration curve away from that obtained from a flat-plate substrate. The dimensionless cutsize that corresponds to 50% penetration, Sqrt(St_{50}) (14), by particles that impact on a porous substrate can be expressed as

$$\sqrt{St_{50}} = \frac{1}{2}\sqrt{1 - 2E_f f_a} \tag{1}$$

$$f_a = 0.695\rho V D_s^{0.9}/\mu L K D_n^{0.9} \tag{2}$$

$$St = \rho_p C D p^2 V/9\mu D_n \tag{3}$$

where f_a represents the additional fraction penetration of the stream into the substrate, E_f is the filtration efficiency by the substrate, D_n is the jet diameter, K is the resistance factor of the sintered stainless-steel filter, V is the air velocity at the jet, μ is the air viscosity, L is the thickness of the sintered stainless-steel filter, D_s is the diameter of the sintered stainless-steel filter, C denotes the Cunningham slip correction factor, ρ_p is the particle density, and D_p is the particle diameter.

The theoretical model for the dimensionless cutsize is based on the following general assumptions.

(a) Flow inside the jet is uniform plug flow parallel to the axis of the jet,
(b) Particle concentration is uniform and particles have the same velocity and direction as the flow,
(c) Radial deposited position for particles that impact on the porous filter equals to the jet radius, and
(d) Filtration efficiency of the particles that penetrate into the substrate equals to 1.

EXPERIMENTAL METHODS

The penetrations of particles that impact on a sintered stainless-steel filter or an aluminum foil substrate were investigated experimentally. Figure 1

schematically depicts the impinging system. This investigation focuses the dimensionless cutsize-shift associated with the particles that impact on a sintered stainless-steel filter. Figure 2 depicts the experimental setup. Oleic acid particles with the aerodynamic diameter ranging from 1 to 10 μm were generated by using an ultrasonic atomizing nozzle (Ultrasonic nozzle, Model 8700, Sono-Tek Inc., NY, USA). The aerosols were dried in the upper section of the test chamber by mixing with dried filtered air and were further neutralized in the middle section. An aerodynamic particle sizer (APS, TSI Model 3310A) was employed to measure the aerosol number concentrations at the inlet and outlet of a sampler installed in the lower section of the test chamber to determine the particle penetration. The test chamber was made of acrylic material. The outside diameter is 40 cm and the total height is 230 cm.

In the sampler, a particle-laden air is passed through a singular jet and directed against an impaction substrate (a sintered stainless-steel filter or an aluminum foil). The impaction model used in this study included one stage impaction plate and a singular jet. The schematic diagram of the impactor with sintered stainless-steel filter is also shown in Fig. 2. The design parameters were determined based on the previous study (16). Two jet diameters of 0.26 cm and 0.36 cm were tested in this study. The distance between the exit of the jet and the top of the impaction substrate (a sintered stainless-steel filter or an aluminum foil) was 0.52 cm and 0.36 cm, respectively. Particle wall loss in the inner wall of the impaction system was measured using monodisperse oleic acid particles tagged with fluorescein. After a sampling period of 5 min, the particles on the impaction substrate,

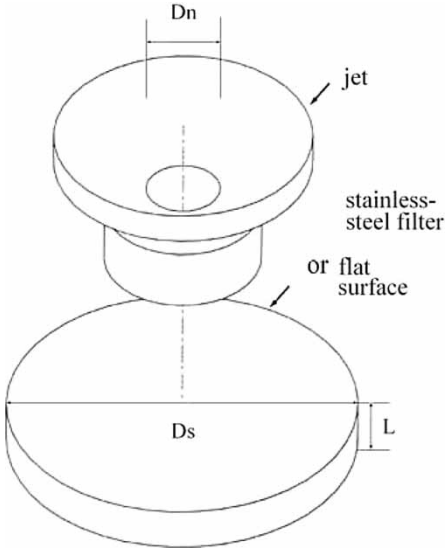

Figure 1. Schematic diagram of impinging system.

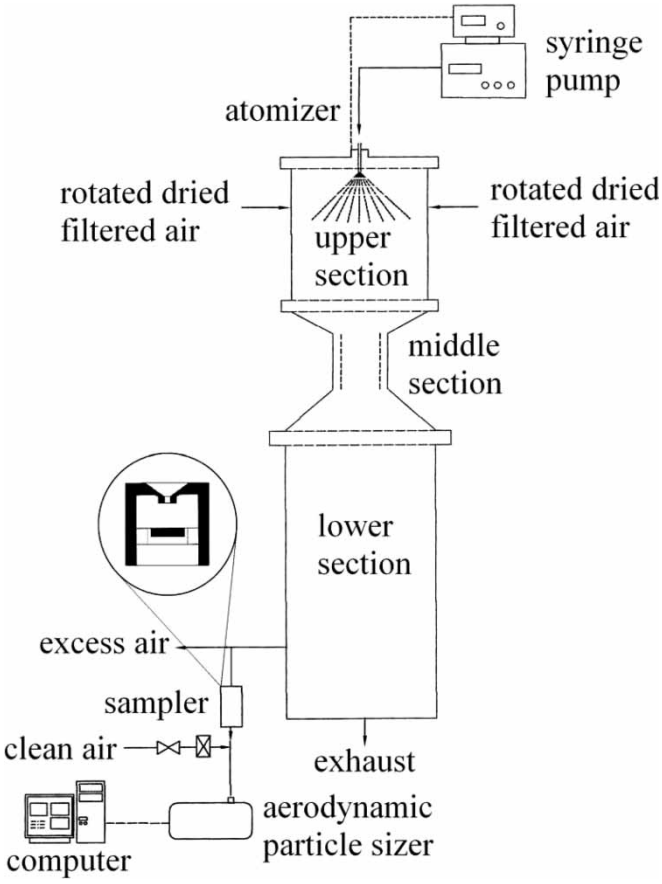

Figure 2. Experimental setup for particle penetration.

the downstream filter, the inner wall, the nozzle, and the other portions of the impactor were extracted by using 0.001 N NaOH. A fluorometer (Model 10-AU, Turner Designs, CA, USA) was used to measure the wall loss of the impaction system. The particle wall loss in the impaction system was found to be less than 4%. Since particle wall loss is small, it is not expected to affect the penetration measurement. Stainless-steel porous filters made by Mott Metallurgical Corp. (Farmington, CT, USA) were used as the impaction substrates. The stainless-steel filter was 0.317 cm in thickness, 1.2 cm in diameter and 100, 40, and 5 μm in pore size. The resistance factor of the stainless-steel filter was determined from the measured pressure drop across the substrate at various flow rates. It was found to be $4.94 \times 10^5\ \mathrm{cm}^{-2}$, $4.06 \times 10^6\ \mathrm{cm}^{-2}$, and $6.87 \times 10^6\ \mathrm{cm}^{-2}$ for pore sizes of 100 μm, 40 μm, and 5 μm, respectively. An aluminum foil substrate with the thickness of 0.005 cm was also tested and employed to simulate a flat-plate substrate.

In the test, the inlet aerosol number concentration (N_1) was sampled at the flow rates from 1.5 to 4.5 L/min without installing the impaction substrate in the sampler first. An additional $0.5 \sim 3.5$ L/min of clean air was added to make the total flow rate of 5.0 L/min for the APS. The outlet aerosol number concentration (N_2) was determined by the APS when the impaction substrate was put in place in the sampler using the same sampling flow rate as the inlet concentration measurement. The duration of each sampling was maintained at 20 seconds, and a wait of 10 seconds was required before the downstream concentration was measured when the substrate was inserted. After the outlet concentration had been measured, the inlet concentration was measured again to check the steadiness of aerosol concentration. The steadiness of the generated particle concentration was found to be within 5%, which was not expected to affect the penetration measurement. One data point at a particular test condition and particle size is the average of six measurements. The penetration of particles, P(%), was determined as:

$$P(\%) = \frac{N_2}{N_1} \times 100\% \tag{4}$$

After the test, the experimental data of penetration for particles that impact on the substrates was fitted by the following expression:

$$P(\%) = A_1 + (A_2 - A_1)/(1 + e^{(D_p - A_3)/A_4}) \tag{5}$$

where A_1, A_2, A_3 and A_4 are regression constants. This equation was utilized to obtain the cutsize of the particle penetration curve.

RESULTS AND DISCUSSION

Penetration by Particles

Figure 3 displays the measured penetration, P(%), of particles that impact on aluminum foil or sintered stainless-steel filters with various pore sizes, from a jet with a diameter of 0.26 cm at a flow rate of 3.0 L/min. Each error bar represents the standard deviation of six experiments. The figure demonstrates that the penetration curves of sintered stainless-steel filters with pore sizes of 100 μm and 40 μm are lower than that of the aluminum foil substrate. This is because the resistance factor of the stainless-steel porous filter decreases with an increasing pore size, resulting in more air penetration into the stainless-steel porous filter. Penetrating air flow causes particles to be collected by the stainless-steel porous filter due to additional particle inertial force and filtration mechanisms. Larger pore sizes and increased roughness of the stainless-steel porous filter also result in higher particle collection efficiencies than the aluminum foil substrate (11). In comparison, for the porous filter with the pore size of

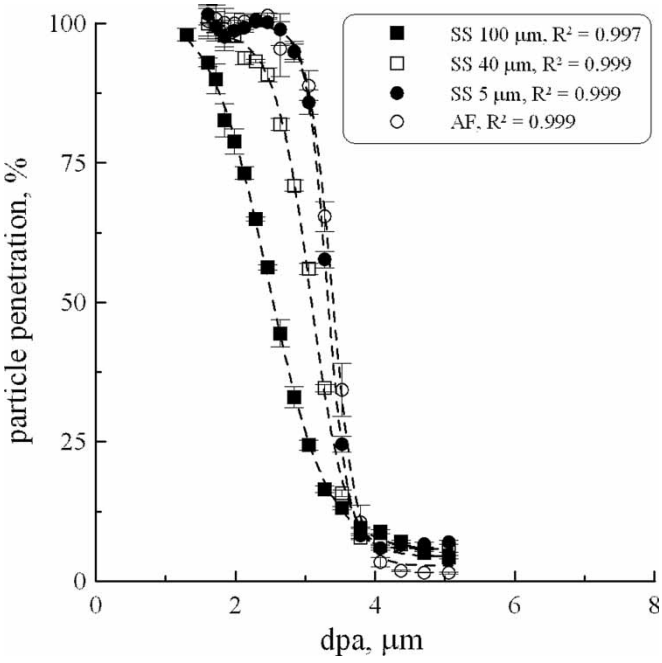

Figure 3. Particle penetration for aluminum foil (AF) and sintered stainless-steel filter (SS) of different pore sizes, flow rate: 3 L/min, jet diameter: 0.26 cm.

5 μm, less air flow penetration into the substrate due to its higher resistance factor, leading to similar penetration curves as that of the aluminum foil substrate. Similar results are observed for the jet diameters of 0.36 cm at the flow rate of 2.5 L/min, as shown in Fig. 4. In both Figs. 3 and 4, the cut-off aerodynamic diameter (the diameter of particle having 50% penetration) for the particles that impinge on the sintered stainless-steel filter is shown to decrease with an increasing pore size. For example, the cut-off aerodynamic diameter is 3.34 μm, 3.11 μm, and 2.56 μm for the pore size of 5 μm, 40 μm, and 100 μm for the flow rate of 3.0 L/min and the jet diameters of 0.26 cm. In comparison, it is 3.40 μm for the aluminum foil substrate at the same condition.

Effect of Re on Particle Penetration

The jet Reynolds number ($Re = \rho V D_n/\mu$, ρ is the air density) has an effect on the particle penetration curve, which is plotted as a function of $Sqrt(St_{50})$ at different Re's numbers for the jet diameter of 0.26 cm in Fig. 5 for the stainless-steel porous filter with pore size = 100 μm. The penetration curve for the aluminum foil substrates is also shown for comparison. Compared to

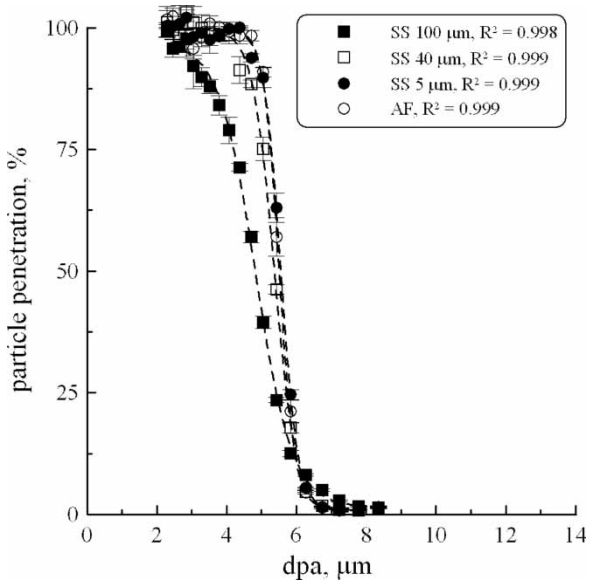

Figure 4. Particle penetration for aluminum foil (AF) and sintered stainless-steel filter (SS) of different pore sizes, flow rate: 2.5 L/min, jet diameter: 0.36 cm.

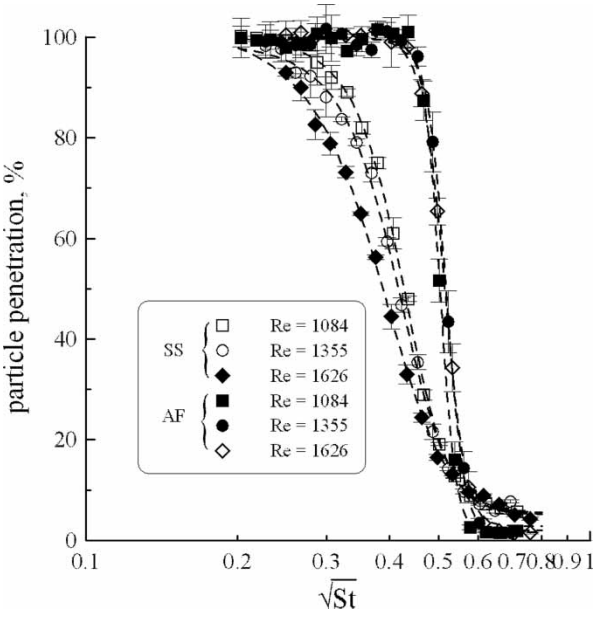

Figure 5. Particle penetration as a function of Sqrt(St) at different Re numbers for the jet diameter of 0.26 cm and the pore size of 100 μm.

the aluminum foil substrate, the penetration curve for the stainless-steel porous filter is shifted to the left and it is less sharp. As Re is increased, there is more of a shift to the left for the penetration curve. The dimensionless cutsize, Sqrt(St_{50}) (Sqrt(St) at 50% penetration) is 0.387, 0.415, and 0.446 for Re = 1626, 1355, and 1084. The sharpness of the penetration curve, S (S = Sqrt(St_{16}/St_{84}), Sqrt(St_{16}) and Sqrt(St_{84}): Sqrt(St) at 16% and 84% penetration) is 1.328, 1,260, and 1.221 for Re = 1626, 1355, and 1084, respectively. Figure 6 displays the particle penetration curve for the jet diameter of 0.26 cm and the pore size of 5 μm at various Reynolds numbers. It indicates that the particle penetration curve for the stainless-steel porous filter is close to that for the aluminum foil substrate. The influence of Re on the penetration curve is not obvious. The previous study indicated that as Re ranged about 1500 ∼ 3000, the collection efficiency curve of impactor was nearly independent of Re whether or not the gravitational effect was considered for a finite impaction plate (17). In addition, the influence of the turbulent transition in the jet on the performance of the impactor was investigated in the literature. The results showed that no transition was observed when the ratio of the nozzle-to-collector distance to the jet diameter equaled 1 or 2, even at Re as high as 2700 (18).

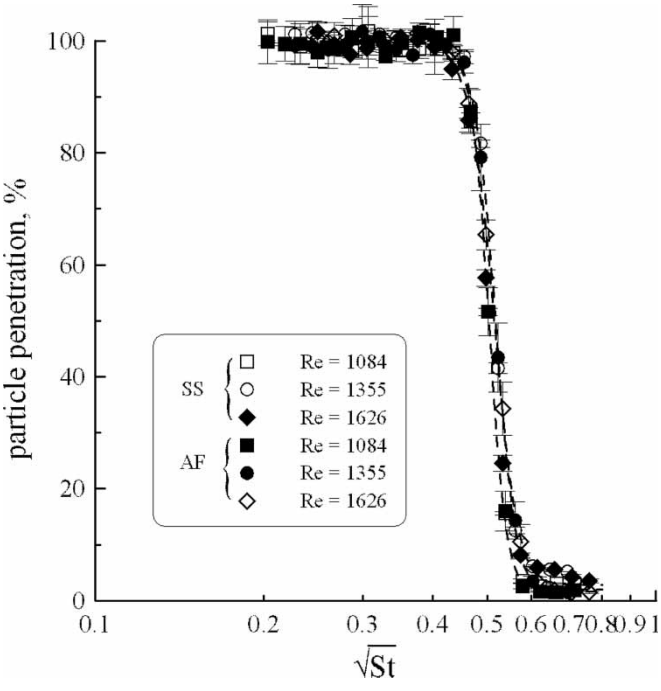

Figure 6. Particle penetration as a function of Sqrt(St) at different Re numbers for the jet diameter of 0.26 cm and the pore size of 5 μm.

Influence of Pore Size

The influence of the pore size on Sqrt(St_{50}) and S can be further explored by evaluating the shift of Sqrt(St_{50}), Sqrt(St_{50})^{shift}, and the shift of sharpness, S_{shift}, for the penetration curve. Sqrt(St_{50})^{shift} and S_{shift} are defined in the following:

$$\sqrt{St_{50}^{shift}} = \sqrt{St_{50_{SS}}}/\sqrt{St_{50_{AF}}} \tag{6}$$

$$S_{shift} = S_{SS}/S_{AF} \tag{7}$$

where the subscripts SS and AF refer to the sintered stainless-steel filter and aluminum foil. Normally, Sqrt(St_{50})$^{shift} < 1.0$ and $S_{shift} > 1.0$ because the dimensionless cutsize of the sintered stainless-steel filter is smaller than the aluminum foil, and the former is less sharp (or larger S) than the latter.

Figures 7 and 8 demonstrate the influence of pore size on the dimensionless cutsize-shift (Sqrt(St_{50})^{shift}) and the sharpness-shift (S_{shift}) for various jet diameters and Re's. Sqrt(St_{50})^{shift} declines as the pore size is increased at the same Re, as shown in Fig. 7. In addition, Sqrt(St_{50})^{shift} falls with an increasing Re number. Decrease of Sqrt(St_{50})^{shift} with an increasing Re is more obvious when the pore size is larger at a fixed Re, Sqrt(St_{50})^{shift} drops in the order of 100, 40, and 5 μm pore size. This is due to more air flow penetration into the

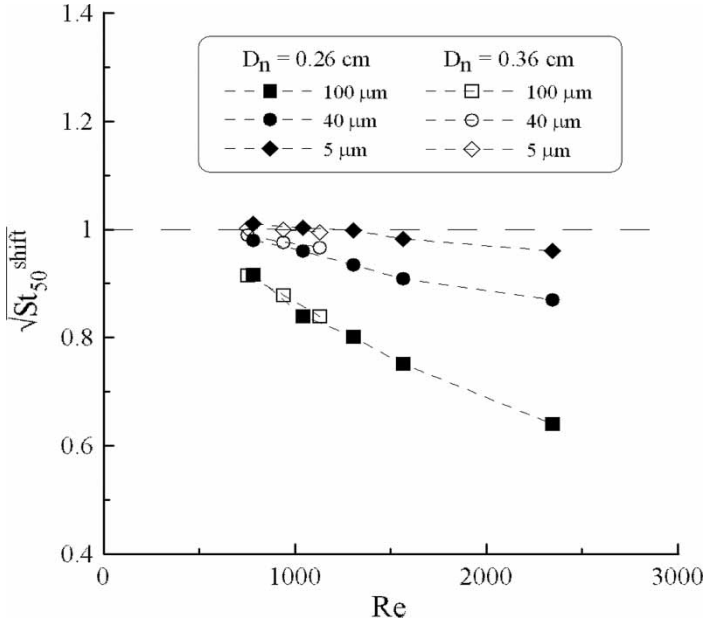

Figure 7. Influence of Re on Sqrt(St_{50})^{shift} for different pore sizes and jet diameters.

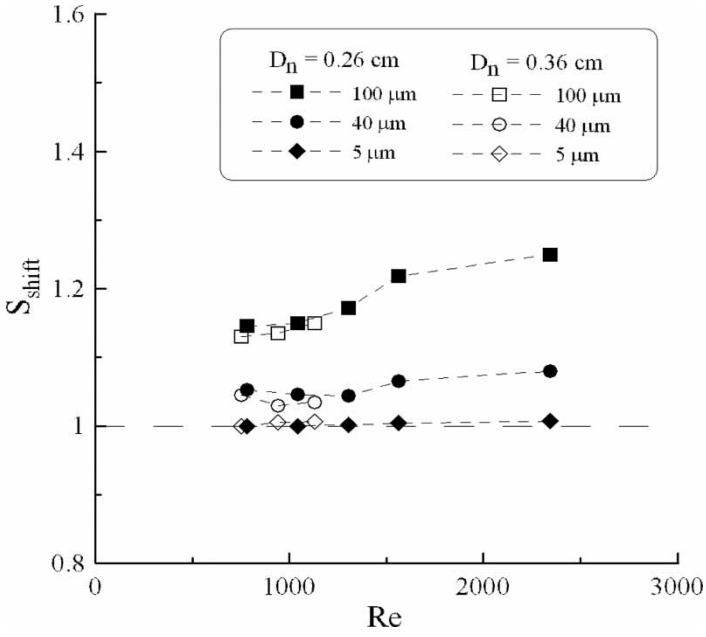

Figure 8. Influence of Re on S_{shift} for different pore sizes and jet diameters.

stainless-steel porous filter as Re is increased for the larger pore sizes. As the pore size is increased, the surface roughness also increases which may increase the collection efficiency and lower the dimensionless cutsize (11). Figure 8 indicates S_{shift} increases as the pore size is increased, indicating that the penetration curve is less sharp for the larger pore size. For the smaller pore size of 5 μm, both $Sqrt(St_{50})^{shift}$ and S_{shift} are close to 1.0, suggesting similar penetration curve with that for the aluminum foil.

Regression Equation for Dimensionless Cutsize-shift

Figure 9 displays the comparison of the experimental data of $Sqrt(St_{50})^{shift}$ with those from the theoretical model. The figure shows that $Sqrt(St_{50})^{shift}$ is close to the theoretical results, and it is independent of Re when f_a is smaller than 0.005. For $f_a > 0.005$, $Sqrt(St_{50})^{shift}$ is seen to decline with an increasing f_a. In such a situation, $Sqrt(St_{50})^{shift}$ will be over-predicted using the theoretical model. For example, the percentage difference between the experimental data and the theoretical results is found to be as high as 28% when $f_a = 0.16$. It is probably due to the influence of the Reynolds number on $Sqrt(St_{50})^{shift}$, which was not considered in the theoretical model. Moreover, the experimental data shown in Fig. 7 indicate that the pore size

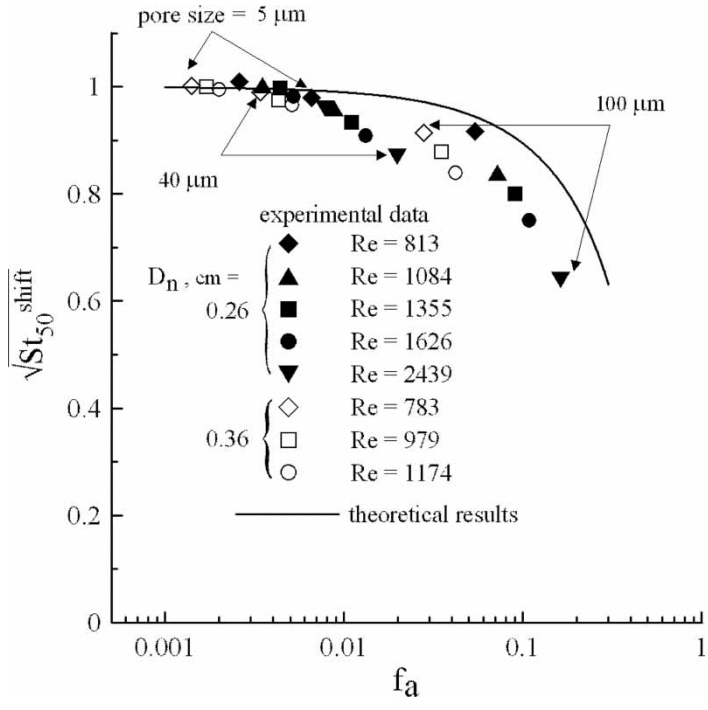

Figure 9. Comparison of experimental data with theoretical results.

of the sintered stainless-steel filter has an effect on $Sqrt(St_{50})^{shift}$. Figure 9 demonstrates the influences of the pore size, the jet diameter and Reynolds number on $Sqrt(St_{50})^{shift}$ will cause three groups in the data, which are deviated from the theoretical model. Besides, the surface roughness of the sintered stainless-steel filter also affected the particle collection efficiencies (11). Accordingly, we decided to fit the present experimental data on $Sqrt(St_{50})^{shift}$, which covers a wide range of pore size ($Ps = 5 \sim 100\ \mu m$), Reynolds number ($Re = 783 \sim 2439$) and additional fraction penetration ($f_a = 0.0014 \sim 0.16$). A regression equation of $Sqrt(St_{50})^{shift}$ was determined by fitting the experimental data using the non-linear multivariable regression technique as:

$$\sqrt{St_{50}^{shift}} = 1/(1 + (0.96f_a + 3 \times 10^{-3}Ps + 1.5 \times 10^{-4}Re)^{2.64}) \quad (8)$$

Figure 10 presents percentage differences from the experimental data of $Sqrt(St_{50})^{shift}$ obtained using the semi-empirical equation, Eq. (8), for various pore sizes. The figure also shows the percentage discrepancy between the experimental data and the theoretical results. The percentage difference between the experimental data and the empirically determined $Sqrt(St_{50})^{shift}$ is $\pm 4\%$, whereas that between the experimental data and the

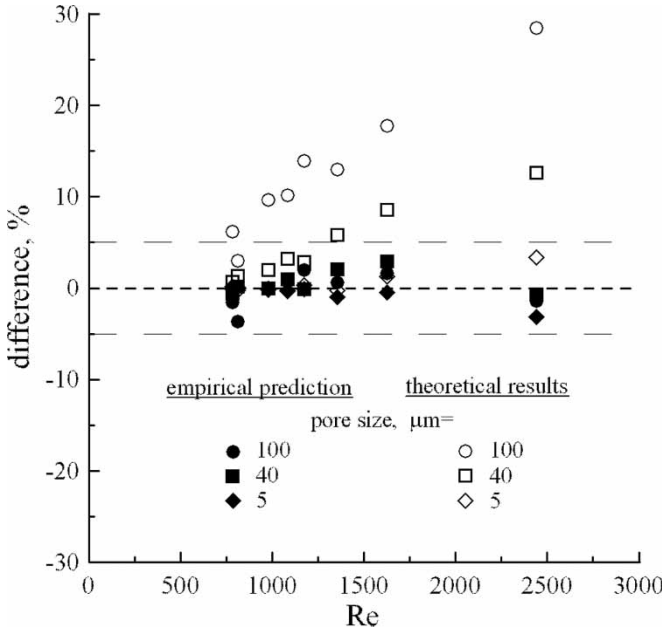

Figure 10. Percentage differences between experimental data and empirical or theoretical results.

theoretical results is as high as 28%. Additionally, the percentage discrepancy increases with Re when the pore size = 100 or 40 μm, according to theory; however, the error in the empirical value remains within 4%. The empirical values of $Sqrt(St_{50})^{shift}$ were further compared with the experimental data, as displayed in Fig. 11. The empirical results are close to the experimental data ($R^2 = 0.998$). Therefore, the regression equation developed herein can be used to predict the dimensionless cutsize for the size-fractionated measurements of particles that impinge on a sintered stainless-steel filter from a singular jet.

CONCLUSIONS

In this work, experimental methods were implemented to obtain the particle penetration curve for particles that impinge on a sintered stainless-steel filter and aluminum foil. Experimental data indicate that the particle penetration, P(%), of the sintered stainless-steel filters with pore sizes of 100 μm and 40 μm are lower and less sharp than those obtained for the aluminum foil substrate, because of such factors as air penetration, flow characteristic, the pore size, and surface roughness of the substrates. For a pore size of 5 μm, the penetration curve is similar to that of the aluminum

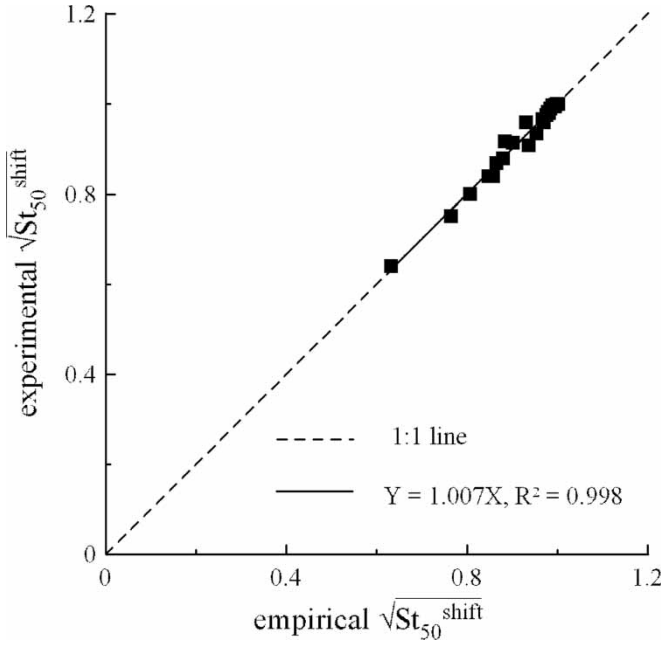

Figure 11. Comparison of empirical results with experimental data.

foil substrate. Experimental data were compared to theoretical results. The theoretical $Sqrt(St_{50})^{shift}$ values follow the same trend as the experimental data, but theory over-predicts the values. Multivariable regression was therefore used to obtain a semi-empirical equation for $Sqrt(St_{50})^{shift}$ by fitting the experimental data. This empirical prediction neglects deviations from the experimental data. The regression equation can be used to predict $Sqrt(St_{50})^{shift}$ for the size-fractionated measurements of particles that impinge on a sintered stainless-steel filter from a singular jet.

ACKNOWLEDGMENTS

The authors would like to thank the National Science Council of the Republic of China, Taiwan, for financially supporting this research under the contract number NSC 92-2211-E-264-005.

REFERENCES

1. Hinds, W.C. (1999) *Aerosol Technology*; Wiley & Sons: New York.

2. John, A.C., Kuhlbusch, T.A.J., and Fissan, H. (1999) Thermodynamic influences on size fractionated measurements (PM2.5, PM10) of ambient aerosols. *J. Environ. Monit.*, 1 (4): 409.
3. Huang, C.H., Chang, C.S., Chang, S.H., Tsai, C.J., Shih, T.S., and Tang, D.T. (2005) Use of porous foam as the substrate of an impactor for respirable aerosol sampling. *J. Aerosol Sci.*, 36 (11): 1373.
4. Dzubay, T.H., Hines, L.E., and Stevens, R.K. (1976) Particle bounce error in cascade impactors. *Atmos. Environ.*, 10 (4): 229.
5. Kenny, L.C., Gussmann, R., and Meyer, M. (2000) Development of a sharp-cut cyclone for ambient aerosol monitoring applications. *Aerosol Sci. Technol.*, 32 (4): 338.
6. Fujitani, Y., Hasegawa, S., Fushimi, A., Kondo, Y., Tanabe, K., Kobayashi, S., and Kobayashi, T. (2006) Collection characteristics of low-pressure impactors with various impaction substrate materials. *Atmos. Environ.*, 40 (18): 3221.
7. Reischl, G.P. and John, W. (1978) The collection efficiency of impaction surfaces: a new impaction surface. *Stuab. Reinhalt. Luft.*, 38 (2): 55.
8. Huang, C.H., Tsai, C.J., and Shih, T.S. (2001) Particle collection efficiency of an inertial impactor with porous metal substrates. *J. Aerosol Sci.*, 32 (9): 1035.
9. Marjamaki, M., Ristimaki, J., Virtanen, A., Moisio, M., Luoma, R., and Keskinen, J. (2000) Testing porous metal substrates in ELPI. *J. Aerosol Sci.*, 31 (S1): S76.
10. van Gulijk, C., Marijnissen, J.C.M., Makkee, M., and Moulijn, J.A. (2003) Oil-soaked sintered impactors for the elpi in diesel particulate measurements. *J. Aerosol Sci.*, 34 (5): 635.
11. Marjamaki, M. and Keskinen, J. (2004) Experimental study on the effect of impaction filter porosity and roughness on impactor collection efficiency. *J. Aerosol Sci.*, 35 (3): 301.
12. Heikkinen, M.S.A. and Harley, N.H. (2000) Experimental investigation of sintered porous metal filters. *J. Aerosol Sci.*, 31 (6): 721.
13. Kim, S., Sioutas, C., and Chang, M. (2000) Electrostatic enhancement of the collection efficiency of stainless steel fiber filters. *Aerosol Sci. Technol.*, 32 (3): 197.
14. Marjamaki, M. and Keskinen, J. (2004) Estimation of the cutpoint of an impactor with porous substrates. *J. Aerosol Sci.*, 35 (5): 657.
15. John, W. (1999) A simple derivation of the cutpoint of an impactor. *J. Aerosol Sci.*, 30 (10): 1317.
16. Huang, C.H. (2005) Predicting cutoff aerodynamic diameter and sharpness of single round-nozzle impactors with a finite impaction plate diameter. *J. Air & Waste Manage., Assoc.*, 55 (12): 1858.
17. Huang, C.H. and Tsai, C.J. (2002) Influence of impaction plate diameter and particle density on the collection efficiency of round-nozzle inertial impactors. *Aerosol Sci. Technol.*, 36 (6): 714.
18. Gómez-Morenoa, F.J., Rosell-Llompart, J., and Fernández de la Mora, J. (2002) Turbulent transition in impactor jets and its effects on impactor resolution. *J. Aerosol Sci.*, 33 (3): 459.